Manufacture-Oriented Design Optimisation of a Flow Diverter Stent Using Lattice Boltzmann Method and Simulated Annealing

Mingzi Zhang[1], Hitomi Anzai[2], Bastien Chopard[3], Makoto Ohta[4]

[1] Graduate School of Engineering, Tohoku University, Sendai, Japan, mingzi.zhang@biofluid.ifs.tohoku.ac.jp
[2] FRIS, Tohoku University, Sendai, Japan, anzai@biofluid.ifs.tohoku.ac.jp
[3] CUI, University of Geneva, Geneva, Switzerland, bastien.chopard@unigh.ch
[4] IFS, Tohoku University, Sendai, Japan, ohta@biofluid.ifs.tohoku.ac.jp

1. Abstract

Background: Flow diverter (FD) intervention is becoming increasingly popular for treatment of cerebral aneurysms (CAs), but post-stenting complications such as delayed rupture and post-stenting stenosis are frequently reported.

Purpose: To reduce the risk of post-stenting complications, we designed an optimisation method for a practical FD composed of 3D helix-like wires using intra-aneurysmal maximum velocity (AMV) as the optimisation objective.

Method: Random modification was performed at each stage to assign a slight change to the starting phase of an arbitrarily selected sub-wire, followed by computational fluid dynamics simulation to model the corresponding haemodynamic behaviours. The optimisation process employed a combination of lattice Boltzmann fluid simulation and simulated annealing. The method was applied to two idealized aneurysm geometries: the straight (S) and curve (C) models.

Results: We evaluated the flow reduction R_f by measuring the AMVs before and after design optimisation with respect to the non-stented case. The R_f of the FD in the S model showed an improvement from 83.63 to 92.77%, and the R_f for the C model increased from 92.75 to 95.49%, both having reached a pre-defined convergence status. By visualizing the streamlines entering an aneurysm after optimisation, we found that an efficient FD design may be closely associated with the disruption of the bundle of inflow by strut placement inside inflow area.

Conclusions: The method improved the flow-diverting performance of an FD while maintaining its original porosity and helix-like structure. This study has provided a design optimisation method for the most commonly used helix-like FD devices.

2. Keywords: cerebral aneurysm, flow diverter, design optimisation, computational fluid dynamics.

3. Introduction

Flow diverter (FD) intervention as an emerging endovascular treatment for cerebral aneurysms (CAs) is attracting growing interest among both clinicians and medical engineers. By blocking aneurysmal inflow, FD intervention is intended to induce thrombotic occlusion inside aneurysms and eventually lead to local haemodynamic rehabilitation. However, clinical reports reveal that complications including post-stenting stenosis and delayed CA rupture frequently occur, and further studies suggest that such complications are closely associated with FD structure design [1–4].

Tominaga et al. observed that post-stenting in-stent stenosis was associated with a high metal-to-arterial tissue ratio of a stent [5], and Lieber et al. and Rhee et al. have shown that the porosity level of FD devices in modifying post-stenting haemodynamic is crucial [3,6]. These studies suggested that an FD design with high flow-diversion efficiency and proper porosity level could avert in-stent stenosis. As to delayed CA rupture, a previous study indicated that a concentrated inflow jet and small impingement regions may lead to rupture [7,8], whereas an increased maximum velocity inside the CA due to FD intervention may be a factor in impingement formation. Thus, an FD design reducing intra-aneurysmal maximum velocity (AMV) can likely contribute to the prognosis of FD intervention.

Recently, the technique of design optimisation has been introduced to achieve an optimally designed FD device for a given CA geometry. Srinivas et al. and Lee et al. performed FD optimisation studies using the exploration of design space approach [9,10], and Anzai et al. studied the optimal FD strut placement for different shapes of CAs using simulated annealing (SA) [11]. These studies have practically shown that optimisation of FD structure can effectively improve device performance from the viewpoint of hemodynamics. However, a manufacture-oriented optimisation strategy that could be applied to the commonly used FD composed of

helix-like woven wires has not yet been performed.
The purpose of this study is to develop an optimisation method for helix-like FD structures to reduce the AMV inside CAs. Based on the combination of LB fluid simulation and SA, this optimisation method automatically identifies optimal FD wire configurations corresponding to a given aneurysm geometry. In view of the correlation between device porosity and in-stent stenosis, we ensured that the porosity was maintained at the high level of 80% by appropriate design of the modification objective. The method can deal with FD devices composed of helical wires and can be flexibly integrated with modern FD manufacturing processes when patient-specific FD fabrication is desired.

4. Methods

4.1. Aneurysm and FD Models

Different vascular geometries produce different aneurysmal inflow characteristics. As suggested by our previous study [11], the intra-aneurysmal hemodynamics differs markedly when the same aneurysm geometry is coupled with different configurations of the parent artery. To investigate the feasibility of the proposed optimisation method under different haemodynamic conditions, two configurations of idealized vascular geometry were used: a straight (S) and curved (C) model. Both models used an aneurysmal diameter of 4.8 mm with a neck diameter of 2.8 mm. The diameter of the parent artery and the curvature radius of the C model were defined as 3.5 and 6.0 mm, respectively.
Each FD was assumed to comprise 8 helix-like woven wires: four clockwise and four anticlockwise wires with strut thickness and width both of 50 μm. The mathematical description of an FD helix trajectory was generated in accordance with the given vascular model and expressed as follows:

$$Clockwise\ helix: \begin{cases} x = [R + r * sin(\omega_\alpha + \theta_n)] * cos\left(\omega_\beta\right) \\ y = [R + r * sin(\omega_\alpha + \theta_n)] * sin\left(\omega_\beta\right) \\ z = r * \cos(\omega_\alpha + \theta_n) \end{cases}, \quad \theta_n = 2(n-1) \cdot \frac{\pi}{4} \tag{1}$$

$$Anticlockwise\ helix: \begin{cases} x = [R + r * cos(\omega_\alpha + \theta_m)] * cos\left(\omega_\beta\right) \\ y = [R + r * cos(\omega_\alpha + \theta_m)] * sin\left(\omega_\beta\right) \\ z = r * sin(\omega_\alpha + \theta_m) \end{cases}, \quad \theta_m = 2\left(m - \frac{1}{2}\right) \cdot \frac{\pi}{4} \tag{2}$$

where r and $\theta_{n\ or\ m}$ denote the radius and starting phase of a helix, respectively, R represents the curvature radius of a helix and ω_α and ω_β are parameters associated with the length and pitch of the helix. To mimic the commonly applied FD stent with homogeneous wire configurations, we created an initial FD structure with uniform helix arrangements: $n\ or\ m \in (1,2,3,4)$ indicates the sequence of either the four clockwise (n) or the four anticlockwise (m) helical subsets. The helix radius r was set as 1.7 mm. In this manner, a deployed FD stent with its struts clinging to the wall of the parent artery was created. As determined by the FD parameters described above, the porosity of the deployed FD was 80%.

4.2. Random Modification

The random modification was designed to alter slightly the relative positions of the eight helices without changing the device porosity. At each stage of optimisation, the random modification function was invoked once. It arbitrarily selected one of the eight helices and added a stochastic variable $\Delta\theta \in \left(-\frac{\pi}{8}, \frac{\pi}{8}\right)$ to the starting phase, the design variable, of the selected helix:

$$\theta_{n\ or\ m,current} = \theta_{n\ or\ m,previous} + \Delta\theta \tag{3}$$

In this manner, the one-step modification caused an axial displacement of the selected helix along the centre line of the parent artery. In this study, we just modified the starting phase $\theta_{n\ or\ m}$ and left other parameters defining a helix unchanged.

4.3. Lattice Boltzmann (LB) Simulation

LB fluid simulation was used as the CFD solver in our study. LB is a mesoscopic approach that simulates the time and space evolution of kinetic quantities using a particle-distribution function $f_i(r,t)$. The index i denotes the possible lattice directions, running from zero to the lattice coordinate number of the chosen lattice topology; r and t represent discrete positions on a regular lattice and discretised time steps, respectively [12]. Fluid in LB simulation is described in terms of the density distribution of idealized fluid particles moving and colliding on a regular lattice. The collision-propagation dynamic process can be written as

$$f_i(r + \Delta t v_i, t + \Delta t) = f_i(r,t) + \frac{1}{\tau}\left(f_i^{eq} - f_i\right) \tag{4}$$

where f^{eq} and τ are the so-called local equilibrium distribution and relaxation time, respectively.
Here we used D3Q19 lattice topology for 3D steady flow simulation. Bounceback rule was applied to define the non-slip boundary and FD wires. After sensitivity tests, the spatial discretization (Δr) was set at 0.05 mm, corresponding to fluid cell quantities of 3.57×10^6 and 3.01×10^6 for the S and C models, respectively. In a previous study [11], blood flow was assumed to be an incompressible Newtonian fluid and to have a constant velocity of 0.23 m/s at the inlet, giving the same Reynolds number (Re) of 200 for both cases. Velocity was defined with parabolic profiles at inlets and a constant pressure boundary was imposed at outlets. Constant density and kinematic viscosity were assumed to be 1040 kg/m^3 and $4.0 \times 10^{-6} \text{ m}^2/\text{s}$, respectively. Based on the above definition, the kinetic viscosity of the lattice (ν_{LB}) was chosen as 0.012, giving a relaxation time τ of $(6\nu_{LB} + 1)/2$ = 0.536. We used the open source LBM library Palabos version 1.4 [13] for its high flexibility and parallelism.

4.4. Simulated Annealing
The same cooling schedule of SA that we previously developed [11] was employed to control random modifications progressing towards the optimal solution. It was designed to identify the FD structure with the best flow diversion rate within a certain range of temperature drop. The AMV was selected as the objective function of SA.
Optimisation started with a uniform FD structure and ended on reaching the lower temperature limit. We assumed that optimisation experienced 50 temperature decrements and accordingly calculated the lower limits for all cases as shown in Table 1. During each stage of optimisation, stent structure was first modified and then CFD was performed to obtain the corresponding AMV. The LB simulation and the optimisation process were fully automated by building the two parts into one program. On a parallel computing system with 256 cores at the Institute of Fluid Science, Tohoku University, CFD simulations of the S and C models required approximately 30 min and 45 min, respectively.

Table 1: Initial temperature and lower temperature limits of SA for the S and C models.

	S model	C model
Initial temperature	2.414×10^{-3}	6.636×10^{-4}
Lower temperature limit	1.244×10^{-5}	3.420×10^{-6}

4.5. Flow reduction rate
To evaluate quantitatively the flow diversion efficiency of the FD device, we introduced a dimensionless index of flow reduction (FR) rate,

$$R_f = \frac{V_{w/o} - V_{current}}{V_{w/o}} \times 100\% \tag{5}$$

where $V_{w/o}$ is the AMV without FD intervention and $V_{current}$ is the AMV calculated after FD implantation of a given wire configuration.

5. Results
The optimisation procedure required 913 and 908 SA iterations for the S and C models, respectively, until the lower temperature limits were reached. No further FR improvement of AMV was obtained during the final 100 iterations for both cases. Compared with the initial uniform FD interventions, the R_f values of optimized FD interventions were improved by 9.12% and 2.74% for the S and C models, respectively. The AMV and R_f under non-stent, initial stent and optimized FD intervention for both models are shown in Table 2.

5.1. Optimisation Process
Figure 1 shows the SA processes of both cases. The R_f of the S model increased during the initial 400 iterations, rising from around 84% at iteration 0 to approximately 92% at iteration 400 before stabilizing at 92%. For the C model, the R_f fluctuated between 92% and 88% during the initial 200 iterations before the best R_f of 95.49% was finally achieved. The models showed a similar trend, by which R_f increased during the first hundreds of iterations and then stabilized.

5.2. FD Structures and Haemodynamic Differences
Figure 2 shows the FD structures and the haemodynamic differences between the initial and the optimized FDs. As can be observed in both cases, the FD wires had a tendency of concentrating at the inflow proximal end. The homogeneous wire structures were disrupted and large holes could be observed in the optimized FD structures. Compared with the initial FD intervention, the magnitude of velocity components perpendicular to the

aneurysmal orifice markedly decreased, particularly in the inflow area, after optimized FD intervention. The isovelocity surfaces, colour-coded by velocity magnitude, corresponded to 0.01 and 0.015 m/s for the S and C models, respectively. As visualized from the isovelocity surface in the optimized case, the flow region with high velocity magnitude was reduced in the aneurysmal orifice compared with that in the initial case.

Table 2: The AMV and the R_f under non-stent, initial stent and optimized FD conditions of S and C models, respectively.

	Non-stent	Initial stent placement		Optimal stent placement	
	$V_{w/o}$ $(10^{-3}m/s)$	$V_{initial}$ $(10^{-3}m/s)$	$R_f(\%)$	$V_{optimal}$ $(10^{-3}m/s)$	$R_f(\%)$
S model	36	6.131	83.63	2.610	92.77
C model	145.828	10.560	92.75	6.567	95.49

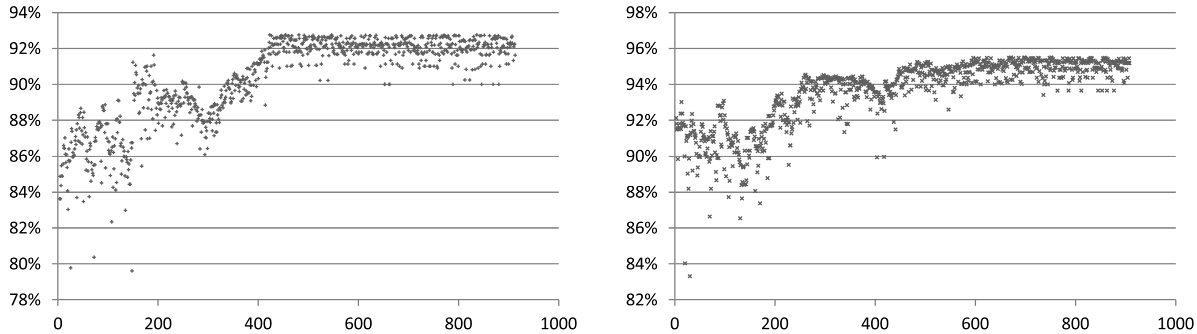

Figure 1: SA process for S and C models. (Left: S model, right: C model, horizontal coordinate: SA step and vertical coordinate: FR rate)

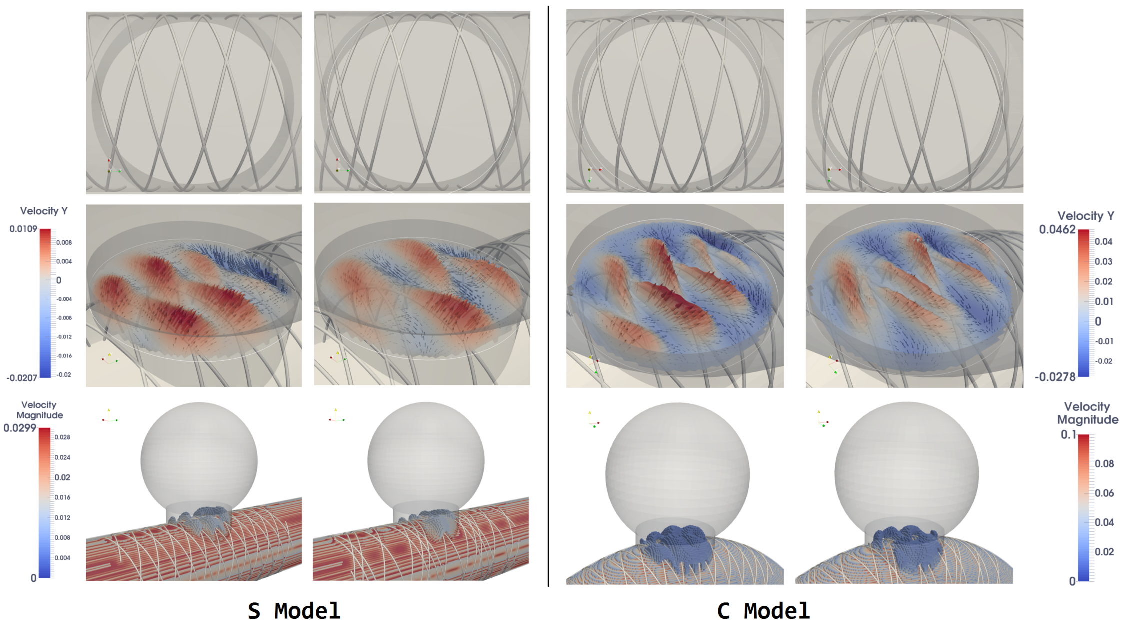

Figure 2: The initial/optimized FD structures (top), the visualization of velocity components perpendicular to the neck plane (middle) and the isovelocity surfaces (bottom) for S and C models. The left and right columns in the S/C models correspond to the initial and the optimized FD interventions, respectively.

5.3. Alteration of intra-aneurysmal average velocity (AAV) reduction rate

Figure 3 shows the alteration of AAV with respect to AMV during the optimisation process. As can be observed in the figure, an FR improvement of AMV did not accompany that of AAV. For the S model, the highest R_f of 92.77% was obtained, whereas the reduction rate of AAV was only around 93% at this point (refer to point A in Figure 3). The highest reduction rate of AAV was observed as point B (just over 94%), whereas the R_f of AMV was only approximately 87%. For the C model, optimal solutions are observed to concentrate in region C (Figure 3); nonetheless, the maximum reductions of AMV (point D) and AAV (point E) are not at the same point.

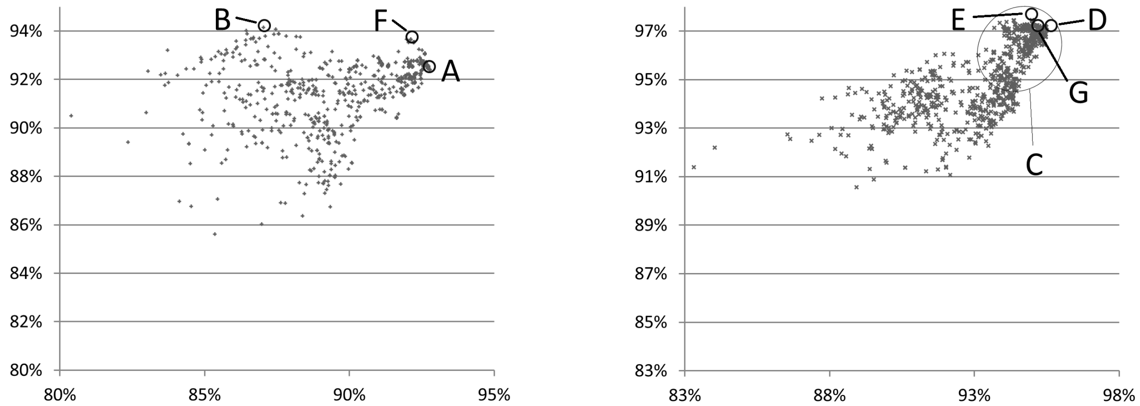

Figure 3: Reduction rates of AMV (horizontal coordinates) and AAV (vertical coordinates) of S model (left) and C model (right), respectively.

6. Discussion

In this study, we performed wire structure optimisation for an FD device composed of helix wires according to two idealized CA geometries. Results suggested that the optimized FD structures had flow-reducing capability superior to the initial uniform structures. The shape of each wire and the woven angle of two arbitrary wires were maintained over the optimisation period, following the intention of introducing minimal alterations to the FD's initial configuration.

6.1. Improving FR Rate by Disrupting the Bundle of Inflow (BOI)

First introduced by Anzai et al. [11,14], disrupting the BOI of a given CA geometry is crucial for increasing the FR rate. BOI refers to the inflow bundle of an aneurysm and can be visualized as the concentrated streamlines that enter an aneurysm. As shown in Figure 4, the width and magnitude of BOI after optimized FD intervention decreased in both S and C models compared with those after initial FD intervention; the FD wires became denser within the BOI zones (refer to the yellow circles with dotted lines in Figure 4). Anzai et al. used AAV as the objective function for optimisation [11], whereas we used AMV in this study. However, the same trend of wire struts concentrating inside the BOI zone after optimisation was observed, confirming the importance of disrupting BOI to obtaining an increased FR rate. Moreover, in the S model, the flow complexity, a flow characteristic associated with CA rupture [7], was observed to decrease after optimisation, with the flow pattern within the aneurysm showing no flow divisions or separations.

6.2. Selecting an Objective Function for Optimisation

Different objective functions lead to different optimisation solutions. Selecting a proper objective function(s) is important for optimisation to identify meaningful modifications. Here we used AMV as the objective function because of its possible correlation with CA ruptures. In addition to AMV, many other haemodynamic parameters (such as AAV, vorticity, wall sheer stress and pressure) have been used for FD structure optimisation in previous studies. Performing optimisation for FD devices is driven by improving treatment prognosis, but no consensus on a critical parameter(s) that can clearly determine the prognosis has yet been reached.

We measured the AAV during the simulation because it is considered to be associated with post-stenting thrombotic occlusion. As observed in Figure 3, an advanced AMV reduction does not always accompany increased AAV reduction. Thus, to achieve an FD structure with both lower AMV and AAV, the FD structures corresponding to point F and G in Figure 3 may be considered as optimal compromise solutions for the S and C models, respectively. Alternatively, optimisation using multiple objective functions can be applied, provided that the critical parameters correlated with short-term thrombotic occlusion or delayed CA rupture can be identified.

7. Conclusion

In this paper, we developed an optimisation method for FD wires with helix-like structure. This method improved the flow-diverting performance of an FD while maintaining its original porosity and helix-like structure. In addition, this study has provided a design optimisation method for the most commonly used helix-like FD devices.

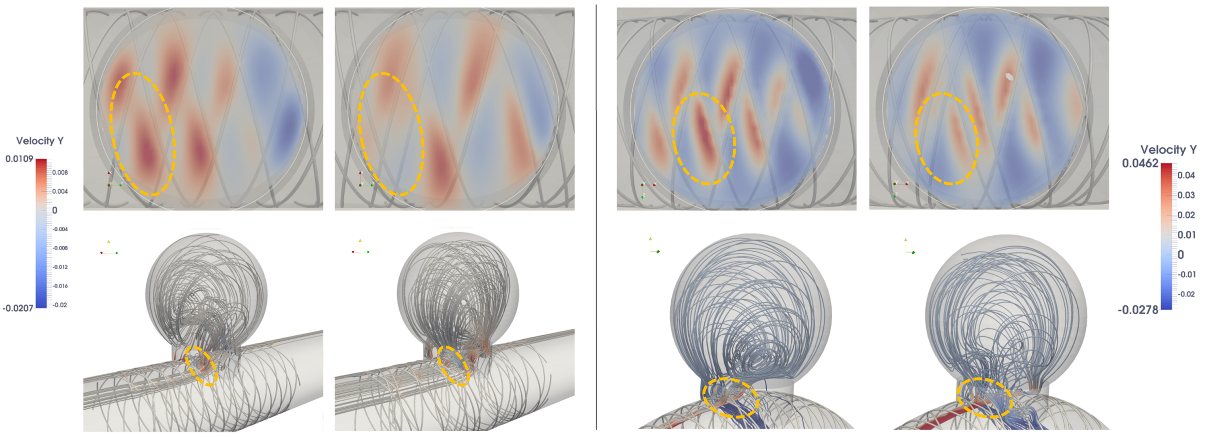

S Model C Model

Figure 4: BOI zones (the yellow circles with dotted lines) alterations after FD structure optimisation. The left and right columns in S/C models correspond to initial and optimized FD interventions, respectively.

8. Acknowledgements

This study was supported by a Grant-in-Aid for Scientific Research (B), Japan Ministry of Education, Science, Sports and Culture, 2013–2015 (25282140, Makoto Ohta) and also in part by the Excellent Graduate Schools program and the JSPS Core-to-Core Program (A. Advanced Research Networks) at the Institute of Fluid Science, Tohoku University, Japan.

9. References

[1] J.E. Cohen, J.M. Gomori, S. Moscovici, R.R. Leker and E. Itshayek, Delayed complications after flow-diverter stenting: reactive in-stent stenosis and creeping stents, *Journal of Clinical Neuroscience*, 21 (7), 1116-1122, 2014.

[2] T. Mattingly, B. Van Adel, E. Dyer, P. Lopez-Ojeda, D.M. Pelz, S.P. Lownie, T. Marotta and M. Boulton, Failure of aneurysm occlusion by flow diverter: a role for surgical bypass and parent artery occlusion, *Journal of NeuroInterventional Surgery*, 7, e31, 2015.

[3] B.B. Lieber, A.P. Stancampiano and A.K. Wakhloo, Alteration of hemodynamics in aneurysm models by stenting: influence of stent porosity, *Annals of Biomedical Engineering*, 25 (3), 460-469, 1997.

[4] S. Appanaboyina, F. Mut, R. Löhner, C. Putman and J. Cebral, Simulation of intracranial aneurysm stenting: techniques and challenges, *Computer Methods in Applied Mechanics and Engineering*, 198 (45-46), 3567-3582, 2009.

[5] R. Tominaga, H. Harasaki, C. Sutton, H. Emoto, H. Kambic and J. Hollman, Effects of stent design and serum cholesterol level on the restenosis rate in atherosclerotic rabbits, *American Heart Journal*, 126 (5), 1049-1058, 1993.

[6] K. Rhee, M.H. Han and S.H. Cha, Changes of flow characteristics by stenting in aneurysm models: influence of aneurysm geometry and stent porosity, *Annals of Biomedical Engineering*, 30 (7): 894-904, 2002.

[7] J.R. Cebral, F. Mut, J. Weir and C.M. Putman, Association of hemodynamic characteristics and cerebral aneurysm rupture, *American Journal of Neuroradiology*, 32 (2), 264-270, 2011.

[8] J.R. Cebral, M.A. Castro, J.E. Burgess, R.S. Pergolizzi, M.J. Sheridan and C.M. Putman, Characterization of cerebral aneurysms for assessing risk of rupture by using patient-specific computational hemodynamics models, *American Journal of Neuroradiology*, 26 (10), 2550-2559, 2005.

[9] K. Srinivas, S. Townsend, C.J. Lee, T. Nakayama, M. Ohta, S. Obayashi and T. Yamaguchi, Two-dimensional optimization of a stent for an aneurysm, *Journal of Medical Devices*, 4 (2), 021003, 2010.

[10] C.J. Lee, K. Srinivas and Y. Qian, Three-dimensional hemodynamic design optimization of stents for cerebral aneurysms. *Proceedings of the Institution of Mechanical Engineers, Part H: Journal of Engineering in Medicine*, 228 (3), 213-224, 2014.

[11] H. Anzai, J.L. Falcone, B. Chopard, T. Hayase and M. Ohta, Optimization of strut placement in flow diverter stents for four different aneurysm configurations. *Journal of Biomechanical Engineering*, 136 (6), 061006, 2014.

[12] S. Succi, *The Lattice-Boltzmann Equation*, Oxford University Press, Oxford, 2001.

[13] www.palabos.org.

[14] H. Anzai, B. Chopard and M. Ohta, Combinational optimization of strut placement for intracranial stent using a realistic aneurysm, *Journal of Flow Control, Measurement & Visualization*, 2 (2), 67-77, 2014.